


Spin and Charge Pumping by a Steady or Pulse-Current-Driven Magnetic Domain Wall: A Self-Consistent Multiscale Time-Dependent Quantum-Classical Hybrid Approach

Marko D. Petrović,¹ Bogdan S. Popescu,² Utkarsh Bajpai,² Petr Plecháč,¹ and Branislav K. Nikolić^{2,*†}

¹*Department of Mathematical Sciences, University of Delaware, Newark, Delaware 19716, USA*

²*Department of Physics and Astronomy, University of Delaware, Newark, Delaware 19716, USA*

 (Received 3 May 2018; revised manuscript received 8 August 2018; published 16 November 2018; corrected 26 November 2018)

We introduce a multiscale framework that combines a time-dependent nonequilibrium Green-function (TDNEGF) algorithm, scaling linearly in the number of time steps and describing quantum-mechanically the conduction electrons in the presence of time-dependent fields of arbitrary strength or frequency, with classical time evolution of localized magnetic moments described by the Landau-Lifshitz-Gilbert (LLG) equation. The TDNEGF+LLG framework can be applied to a variety of problems where current-driven spin torque induces the dynamics of magnetic moments as the key resource for next-generation spintronics. Previous approaches to such nonequilibrium many-body systems (like the steady-state-NEGF+LLG framework) neglect noncommutativity of a quantum Hamiltonian of conduction electrons at different times and, therefore, the impact of time-dependent magnetic moments on electrons leading to the pumping of spin and charge currents. The pumped currents can, in turn, self-consistently affect the dynamics of magnetic moments themselves. Using the magnetic domain wall (DW) as an example, we predict that its motion will pump time-dependent spin and charge currents (on top of the unpolarized dc charge current injected through normal-metal leads to drive the DW motion), where the latter can be viewed as a realization of quantum charge pumping due to the time dependence of the Hamiltonian and the left-right symmetry breaking of the two-terminal device structure. The conversion of ac components of spin current, whose amplitude increases (decreases) as the DW approaches (recedes from) the normal-metal lead, into ac voltage via the inverse spin Hall effect offers a tool to precisely track the DW position along magnetic nanowire. We also quantify the DW transient inertial displacement due to its acceleration and deceleration by pulse current and the entailed spin and charge pumping. Finally, TDNEGF+LLG as a nonperturbative (i.e., numerically exact) framework allows us to establish the limits of validity of the so-called spin-motive force (SMF) theory for pumped charge current by time-dependent magnetic textures—the perturbative analytical formula of SMF theory becomes inapplicable for large frequencies (but unrealistic in a magnetic system) and, more importantly, for increasing noncollinearity when the angles between neighboring magnetic moments exceed approximately 10° .

DOI: [10.1103/PhysRevApplied.10.054038](https://doi.org/10.1103/PhysRevApplied.10.054038)

I. INTRODUCTION

The current-driven dynamics of collinear textures, such as macrospin [1–3], and noncollinear textures, such as domain walls (DWs) [4–8] and skyrmions [9,10], of localized magnetic moments are both a fundamental problem for nonequilibrium quantum many-body physics and a key resource for next-generation spintronics [11–14]. For example, the current-driven spin-torque-induced magnetization dynamics in magnetic tunnel junctions

(MTJs) [1,3] or ferromagnet/spin-orbit-coupled-material bilayers [8,15,16] can implement a variety of functionalities, such as nonvolatile magnetic random access memories (MRAM), microwave oscillators, microwave detectors, spin-wave emitters, memristors, and artificial neural networks [11–14]. The spin torque can also move DWs and skyrmions along magnetic nanowires that underlies racetrack [17,18] and skyrmionic memories [19], respectively, with potentially ultralow energy consumption.

The theoretical analysis of these phenomena requires us to account for the interaction of fast conduction electrons, described quantum mechanically, with slow magnetic moments whose dynamics can be captured by the classical Landau-Lifshitz-Gilbert (LLG) equation

*bnikolic@physics.udel.edu

†Present address: Catalan Institute of Nanoscience and Nanotechnology (ICN2), Campus UAB, Bellaterra, 08193 Barcelona, Spain.

[3,20,21]. However, quantum transport studies of spin torque in spin valves [16,22–24], MTJs [25–27], and DWs [28–34] are typically confined to computing the torque of a steady current of electrons acting on a chosen static configuration of localized magnetic moments. Similarly, standard classical micromagnetic simulations of current-driven magnetization dynamics [2,3] or motion of DWs [7, 8,21,35–41] and skyrmions [42,43] evade explicit modeling of the flow of conduction electrons and, instead, require phenomenological terms to describe the so-called adiabatic (when propagating electron spins remain mostly aligned or antialigned with the localized magnetic moments) and nonadiabatic (which can have local [28–30] and nonlocal [31–33] contributions) spin torques due to flowing electrons. Deriving additional torque expressions is required in the presence of spin-orbit coupling [44,45] or nontrivial topology [46] of magnetic textures [47].

A handful of studies [48–52] have also attempted to develop a multiscale combination of computational quantum (or even simpler semiclassical [53–56]) transport of conduction electrons with a discretized LLG equation for the motion of localized magnetic moments described by the classical vectors $\mathbf{M}_i(t)$. However, these attempts employ a steady-state nonequilibrium density matrix, strictly applicable only to systems that do not evolve in time, which can be expressed in terms of the lesser Green function $\mathbf{G}^<(E)$ of the nonequilibrium Green function (NEGF) formalism [57]

$$\rho_{\text{neq}} = \frac{1}{2\pi i} \int_{-\infty}^{+\infty} dE \mathbf{G}^<(E). \quad (1)$$

Thus, such a NEGF + LLG approach [48–52] naively assumes that electrons respond instantaneously to the time-dependent potential introduced into the quantum Hamiltonian of the conduction electrons by the time evolution of $\mathbf{M}_i(t)$, thereby neglecting noncommutativity of the quantum Hamiltonian at different times. On the other hand, it is well known that even infinitely slow dynamics of $\mathbf{M}_i(t)$ can pump spin currents [58,59], as well as charge current if additional conditions are satisfied [59–61]. Therefore, using the NEGF+LLG approach precludes taking into account self-consistent feedback [55,62], where the dynamics of $\mathbf{M}_i(t)$ leads to pumped spin currents, which, in turn, can exert additional torque and time-retarded damping (with a microscopically [63,64] rather than phenomenologically [65,66] determined memory kernel) on $\mathbf{M}_i(t)$, thereby modifying its dynamics. Finally, the time-dependent quantum treatment of electrons is required to describe the pulse-current-induced dynamics of $\mathbf{M}_i(t)$, which is of paramount importance in basic research experiments [8] and, e.g., racetrack memory applications [17,18]. For example, usage of current pulses [67] or their trains [68] reduces the threshold current density to move the DW,

while precise control of the DW position can be achieved by tailoring the pulse duration and shape [38,69–72].

Taking into account these effects demands that we construct the time-dependent nonequilibrium density matrix, $\rho_{\text{neq}}(t)$. This can be accomplished using the time-dependent NEGF (TDNEGF) formalism [57,73]

$$\rho_{\text{neq}}(t) = \frac{1}{i} \mathbf{G}^<(t, t')|_{t=t'}, \quad (2)$$

where the lesser Green function $\mathbf{G}^<(t, t')$ depends on two times t and t' in arbitrary nonequilibrium situations [57] [in steady-state nonequilibrium, it depends on $t - t'$, so it can be Fourier transformed to energy, as utilized in Eq. (1)]. Within this more general framework, the NEGF+LLG approach corresponds to taking just the lowest order of $\rho_{\text{neq}}(t)$ expanded in power series in small $d\mathbf{M}_i/dt$ [74,75], so that $\mathbf{G}(E)$ and $\mathbf{G}^<(E)$ are assumed to depend only parametrically on time and are effectively computed for the frozen-in-time configuration of $\mathbf{M}_i(t)$. For instance, the neglected first-order correction contains information about the Gilbert damping term in the LLG equation [74,75].

The nonequilibrium density matrix yields an expectation value of any physical quantity, such as the current-driven (CD) part of nonequilibrium spin density:

$$\begin{aligned} \mathbf{S}_{\text{CD}}^i(t) &= \mathbf{S}_{\text{neq}}^i(t) - \mathbf{S}_{\text{eq}}^i \\ &= \frac{\hbar}{2} \text{Tr}_{\text{spin}}[\rho_{\text{neq}}(t)\boldsymbol{\sigma}] - \frac{\hbar}{2} \text{Tr}_{\text{spin}}[\rho_{\text{eq}}\boldsymbol{\sigma}]. \end{aligned} \quad (3)$$

For a given quantum Hamiltonian of a conduction electron subsystem, computing $\mathbf{S}_{\text{CD}}^i(t)$ microscopically generates all relevant spin-torque terms $\propto \mathbf{S}_{\text{CD}}^i \times \mathbf{M}_i$ in the LLG equation for $\mathbf{M}_i(t)$. In Eq. (3), $\boldsymbol{\sigma} = (\hat{\sigma}_x, \hat{\sigma}_y, \hat{\sigma}_z)$ is the vector of the Pauli matrices and one has to subtract [16,76] any nonzero equilibrium spin density (present in the absence of current) by using the NEGF expression for the equilibrium density matrix [57],

$$\rho_{\text{eq}} = -\frac{1}{\pi} \int_{-\infty}^{+\infty} dE \text{Im} \mathbf{G}(E) f(E), \quad (4)$$

where $\mathbf{G}(E)$ is the retarded Green function (GF) in equilibrium and $f(E)$ is the Fermi distribution function (identical for both reservoirs in equilibrium).

In this study, we develop a numerically exact [i.e., equivalent to summing all terms in the previously mentioned power series expansion of $\rho_{\text{neq}}(t)$] approach denoted as TDNEGF+LLG. As explained schematically in Fig. 2, TDNEGF+LLG employs $\rho_{\text{neq}}(t)$ in Eq. (2) to obtain $\mathbf{S}_{\text{CD}}^i(t)$ via Eq. (3), which is then coupled to the LLG equation for $\mathbf{M}_i(t)$, which, in turn, is used to obtain $\rho_{\text{neq}}(t)$ at the next time step.

The paper is organized as follows. The details of the TDNEGF+LLG framework are introduced in Sec. II.

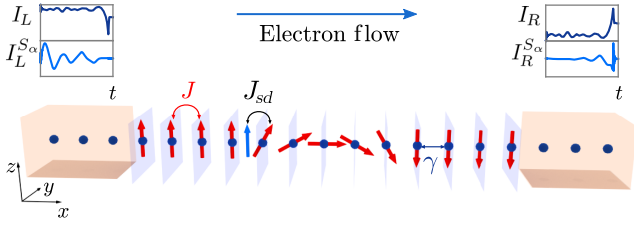


FIG. 1. Schematic view of a magnetic nanowire, hosting a DW formed by noncollinear arrangement of localized magnetic moments (red arrows), which is attached to two normal-metal leads. The DW dynamics is induced by injecting unpolarized charge current from the NM leads, so that electrons become spin polarized as they traverse collinear magnetic moments and exert spin torque on those localized magnetic moments that are noncollinear to their spin-polarization vector (blue arrow). In turn, electrons propagating through a time-dependent potential landscape created by the localized magnetic moments pump time-dependent charge $I_{L,R}(t)$ and spin $I_{L,R}^{S\alpha}(t)$ currents into the leads, which are superimposed on charge and spin currents due to the applied dc or pulse bias voltage. The electronic subsystem is modeled on a tight-binding lattice described by the quantum Hamiltonian in Eq. (8), whereas the localized magnetic moments are described by the classical Hamiltonian in Eq. (6).

To demonstrate the richness of insights made possible by this framework, we apply it to the widely studied [5,7,21,35–41,72] problem of current-driven DW motion along clean magnetic nanowire attached to two normal-metal (NM) leads, where the injected unpolarized charge current from the NM leads is steady in Sec. III or pulsed in Sec. V. In Sec. IV, we employ a toy system of three precessing noncollinear spins to compare nonperturbative results from TDNEGF for a pumped charge current by this system to predictions of a perturbative analytical formula of the so-called spin-motive force (SMF) theory [77,78] for time-dependent magnetization textures, thereby delineating the limits of its validity. We conclude in Sec. VI.

II. TDNEGF+LLG FRAMEWORK

To make the discussion transparent, we use an example of a Néel DW illustrated in Fig. 1 and described by a smooth function [48] of the position x_i of site i along the x axis,

$$\mathbf{M}_i(t=0) = ([\cosh(X_{\text{DW}} - x_i)/W]^{-1}, 0, \times \tanh(X_{\text{DW}} - x_i)/W). \quad (5)$$

Its localized magnetic moments \mathbf{M}_i lie entirely in the plane when the current is zero. Here, X_{DW} is the coordinate of the DW center and $W = 1a$ is its width (in the units of the lattice spacing a). The interaction between localized magnetic moments, whose direction at site i is specified by

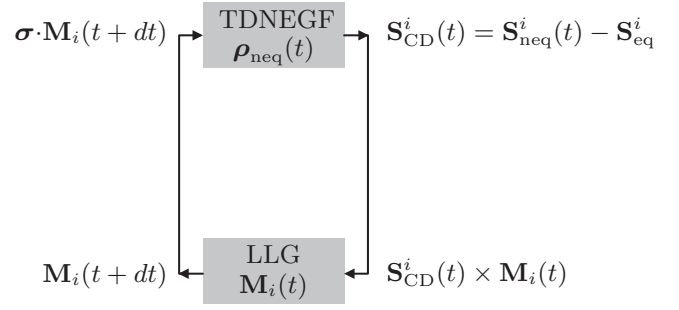


FIG. 2. Scheme of the TDNEGF + LLG self-consistent loop in which TDNEGF calculations supply the current-driven part of electronic nonequilibrium spin density $\mathbf{S}_{\text{CD}}(t)$ defined in Eq. (3). This quantity determines the spin torque entering into the LLG equation for the dynamics of classical vectors \mathbf{M}_i representing localized magnetic moments. In turn, the LLG equations supply the time-dependent s - d interaction term, $\sigma \cdot \mathbf{M}_i(t)$, for the quantum Hamiltonian of the conduction electrons.

unit vector \mathbf{M}_i , while their magnitude is μ_M , is described by the classical Hamiltonian

$$\mathcal{H} = -J \sum_{\langle ij \rangle} \mathbf{M}_i \cdot \mathbf{M}_j - J_{sd} \sum_i \mathbf{S}_{\text{CD}}^i \cdot \mathbf{M}_i - K \sum_i (M_i^z)^2 + D \sum_i (M_i^y)^2. \quad (6)$$

Besides the Heisenberg term with an exchange interaction between the nearest neighbors of strength $J = 0.1$ eV, this Hamiltonian also includes s - d interaction between conduction electrons and localized magnetic moments of strength $J_{sd} = 0.1$ eV, magnetic anisotropy (along the z axis) of strength $K = 0.025$ eV, and demagnetization (along the y axis) of strength $D = 0.029$ meV (corresponding to the demagnetizing field of approximately 1 T). The Hamiltonian in Eq. (6) determines the effective magnetic field acting on each localized magnetic moment, $\mathbf{B}_{\text{eff}}^i = -\frac{1}{\mu_M} \partial \mathcal{H} / \partial \mathbf{M}_i$, which is inserted into the atomistic LLG equation (for simplicity, without the noise term required at nonzero temperature) [20,21,41]

$$\frac{\partial \mathbf{M}_i}{\partial t} = -\frac{g}{1 + \lambda^2} [\mathbf{M}_i \times \mathbf{B}_{\text{eff}}^i + \lambda \mathbf{M}_i \times (\mathbf{M}_i \times \mathbf{B}_{\text{eff}}^i)]. \quad (7)$$

Here, g is the gyromagnetic ratio and the intrinsic Gilbert damping parameter [79] is chosen as $\lambda = 0.01$, as found in many realistic magnetic nanowires [37,38,71]. Such coupled LLG equations are solved by the Heun numerical scheme [20].

The conduction electron subsystem is described by the quantum Hamiltonian for a one-dimensional (1D) tight-binding (TB) model of a magnetic nanowire:

$$\hat{H}_{\text{TB}} = -\gamma \sum_{\langle ij \rangle} \hat{c}_i^\dagger \hat{c}_j - J_{sd} \sum_i \hat{c}_i^\dagger \boldsymbol{\sigma} \cdot \mathbf{M}_i(t) \hat{c}_i, \quad (8)$$

where $\hat{c}_i^\dagger = (\hat{c}_{i\uparrow}^\dagger \ \hat{c}_{i\downarrow}^\dagger)$ is a row vector containing operators $\hat{c}_{i\sigma}^\dagger$, which create an electron with spin $\sigma = \uparrow, \downarrow$ at site i ; \hat{c}_i is a column vector containing the corresponding annihilation operators; and $\gamma = 1$ eV is the nearest-neighbor hopping. The TB chain described by Eq. (8) is attached [Fig. 1] to two semi-infinite NM leads, modeled by the same Hamiltonian in Eq. (8) but with $J_{sd} = 0$. We inject through the NM leads conventional unpolarized charge current using dc bias voltage V_b , applied as an electrochemical potential difference, $\mu_L = E_F + eV_b/2$ and $\mu_R = E_F - eV_b/2$, between the macroscopic reservoirs into which the left (L) and right (R) leads are assumed to terminate. We also use voltage pulses of different shapes (see Fig. 8 for illustration), whose amplitude is the same as the dc bias voltage. We quote the Fermi energy $E_F^b = E_F - E_b$ with respect to the bottom of the band $E_b = -2.0\gamma$ of the NM leads.

The Hamiltonian in Eq. (8) contains a time-dependent term due to $\mathbf{M}_i(t)$ supplied [Fig. 2] by solving the system of LLG equations displayed as Eq. (7). Thus, rigorously, it must be treated by some approach of time-dependent nonequilibrium quantum statistical mechanics, which can yield $\rho_{\text{neq}}(t)$ in Fig. 2. The TDNEGF formalism [57,73] offers a route to $\rho_{\text{neq}}(t)$, as shown in Eq. (2). It operates with two fundamental quantities [57]: the retarded $G_{ii'}^{\sigma\sigma'}(t, t') = -i\Theta(t - t')\langle\{\hat{c}_{i\sigma}(t), \hat{c}_{i'\sigma'}^\dagger(t')\}\rangle$ and the lesser $G_{ii'}^{<\sigma\sigma'}(t, t') = i\langle\hat{c}_{i'\sigma'}^\dagger(t')\hat{c}_{i\sigma}(t)\rangle$ GFs which describe the density of available quantum states and how electrons occupy those states, respectively.

For the device in Fig. 1, we solve a matrix integro differential equation [80,81]:

$$i\hbar \frac{d\rho_{\text{neq}}}{dt} = [\mathbf{H}_{\text{TB}}, \rho_{\text{neq}}] + i \sum_{p=L,R} [\mathbf{\Pi}_p(t) + \mathbf{\Pi}_p^\dagger(t)], \quad (9)$$

which can be viewed as the exact master equation for an open finite-size quantum system, described by \mathbf{H}_{TB} , that is attached via semi-infinite leads to much larger macroscopic reservoirs. We use a convention in which boldface symbols denote matrices in orbital \otimes spin vector space, where the size of the orbital space is equal to the number of sites ($i = 1-50$ is chosen for the central magnetic nanowire region in Fig. 1) and the size of the spin space is two. The matrix

$$\mathbf{\Pi}_p(t) = \int_{t_0}^t dt_2 [\mathbf{G}^>(t, t_2)\mathbf{\Sigma}_p^<(t_2, t) - \mathbf{G}^<(t, t_2)\mathbf{\Sigma}_p^>(t_2, t)], \quad (10)$$

is expressed in terms of the lesser/greater GF and the corresponding lesser/greater self-energies $\mathbf{\Sigma}_p^{>,<}(t_2, t)$ [57], whose numerical construction in order to convert Eq. (9) into a system of ordinary differential equations can be found in Ref. [81]. Equation (10) yields charge current in

lead $p = L, R$ of the device.

$$I_p(t) = \frac{e}{\hbar} \text{Tr}[\mathbf{\Pi}_p(t)], \quad (11)$$

as well as the spin currents,

$$I_p^{S\alpha}(t) = \frac{e}{\hbar} \text{Tr}[\hat{\sigma}_\alpha \mathbf{\Pi}_p(t)]. \quad (12)$$

We use the same units for both types of current, $I_p = I_p^\uparrow + I_p^\downarrow$ and $I_p^{S\alpha} = I_p^\uparrow - I_p^\downarrow$, defined in terms of spin-resolved charge currents I_p^σ for $\sigma = \uparrow, \downarrow$ along the α axis. The local (bond) charge current [82] between sites i and j is computed as

$$I_{i \rightarrow j}(t) = \frac{e\gamma}{i\hbar} \text{Tr}_{\text{spin}} [\rho_{\text{CD}}^{ij}(t) - \rho_{\text{CD}}^{ji}(t)], \quad (13)$$

and the local spin currents are given by

$$I_{i \rightarrow j}^{S\alpha}(t) = \frac{e\gamma}{i\hbar} \text{Tr}_{\text{spin}} [\hat{\sigma}_\alpha \{ \rho_{\text{CD}}^{ij}(t) - \rho_{\text{CD}}^{ji}(t) \}], \quad (14)$$

where the current-driven part of the nonequilibrium density matrix is obtained as $\rho_{\text{CD}}^{ij}(t) = \rho_{\text{neq}}^{ij}(t) - \rho_{\text{eq}}^{ij}(t)$.

The computational complexity of TDNEGF calculations stems from the memory effect—the entire history must be stored in order to accurately evolve the NEGFs. For efficient calculation over long times and for a large number of simulated sites, we employ recently developed TDNEGF algorithms [80,81], which scale linearly [73] in the number of time steps. While we choose in this study 1D systems, so that our results can be compared directly to previous NEGF+LLG studies of DW motion in 1D [48], the TDNEGF+LLG calculations can also be applied to higher-dimensional systems hosting noncollinear textures like skyrmions. To study such systems, the main limitation is the scaling of computational time for TDNEGF calculations with the number of sites N , which is $\sim N$ for a small number of sites $N \lesssim 10^2$, but it becomes $\sim N^3$ for a larger number of sites due to matrix-matrix multiplication in Eq. (9), while maintaining $\sim t$ scaling in time [81]. Other TDNEGF algorithms can scale linearly with both system size and simulation time [83], but they do not provide directly $\rho_{\text{neq}}(t)$ at each time step.

We also compare our TDNEGF+LLG framework to related recent efforts toward hybrid time-dependent-quantum/time-dependent-classical descriptions of systems where conduction electrons interact with classical localized magnetic moments. Such an approach introduced in Ref. [63] has the same feedback loop illustrated in Fig. 2, but it considers electronic subsystems as a closed quantum system (e.g., as described by a finite length TB chain [63]) whose master equation in Eq. (9), therefore, does not contain a second term on the right-hand side. This

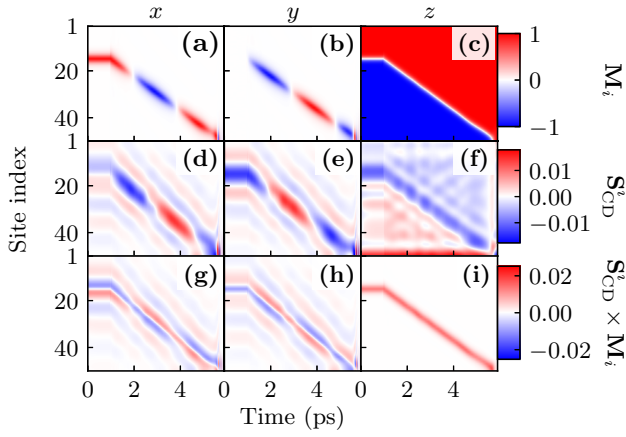


FIG. 3. Spatiotemporal profiles of the components of (a)–(c) localized magnetic moments $\mathbf{M}_i(t)$; (d)–(f) current-driven nonequilibrium spin density $\mathbf{S}_{\text{CD}}^i(t)$, defined in Eq. (3); and (g)–(i) spin torque $\mathbf{T} \propto \mathbf{S}_{\text{CD}}(t) \times \mathbf{M}_i(t)$ acting on the localized magnetic moments. The Fermi energy is $E_F^b = 0.05$ eV, s - d interaction between conduction electrons and localized magnetic moments is $J_{sd} = 0.1$ eV, and the applied dc bias voltage is $eV_b = 0.05$ eV. The profiles are steady (after transient time following switching of dc bias voltage at $t = 0$) for $t < 1$ ps, where DW is fixed at $X_{\text{DW}} = 15$, but they become time dependent after coupling to LLG dynamics is turned on for $t \geq 1$ ps.

makes it unsuitable for the modeling of spintronic devices where one has to inject or collect spin and charge current through the attached semi-infinite leads. They also play an essential role by converting the discrete spectrum of the central region into a continuous one, which ensures that current reaches a steady state in the long time limit after dc bias voltage is applied, even without explicit modeling of inelastic scattering processes. The approach of Ref. [64] does include semi-infinite leads and macroscopic reservoirs into which they terminate, but it executes a variety of approximations to make possible the analytical solution for junctions containing a single classical localized spin, so it is not suitable for spatially extended spintronic devices with many coupled classical spins, which require numerical modeling. The quantum part of both approaches [63,64] generates effectively a non-Markovian LLG equation due to additional time-retarded damping, on top of intrinsic Gilbert damping (arising from the combined effects of spin-orbit coupling and electron-phonon interaction [79]) that we take into account by using nonzero λ in Eq. (7). Our TDNEGF+LLG framework also contains time-retarded damping whose memory kernel properties will be discussed in future studies.

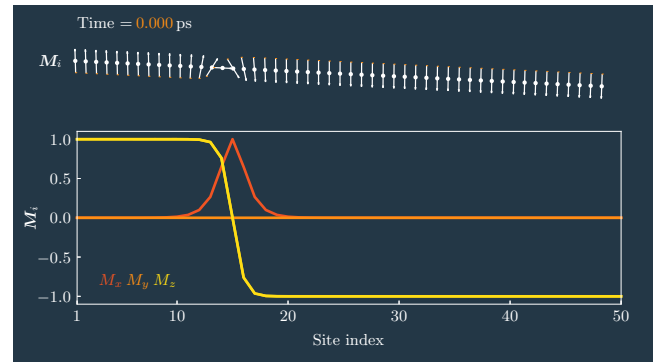
III. DW MOTION DRIVEN BY STEADY CURRENT: SPIN AND CHARGE PUMPING

Evolving $\rho_{\text{neq}}(t)$ via Eq. (9) requires time step $\delta t = 0.1$ fs for numerical stability. The spatiotemporal profile of

$\mathbf{S}_{\text{CD}}^i(t)$ shown in Figs. 3(d)–3(f) is obtained by plugging in thus evolved $\rho_{\text{neq}}(t)$ into Eq. (3). This profile is supplied to a system of LLG equations for $\mathbf{M}_i(t)$, whose spatiotemporal profile is shown in Figs. 3(a)–3(c), where we use the same time step $\delta t = 0.1$ fs. The noncollinearity at a given time between \mathbf{S}_{CD}^i [Figs. 3(d)–3(f)] and \mathbf{M}_i [Figs. 3(a)–3(c)] generates spin torque $\mathbf{T} \propto \mathbf{S}_{\text{CD}}^i \times \mathbf{M}_i$ on the DW (T_x and T_z determine the dampinglike torque and T_y determines the fieldlike torque [1,16]) whose spatiotemporal profile is shown in Figs. 3(g)–3(i). Figure 3(b) and Video 1, showing the complete time evolution of $\mathbf{M}_i(t)$, demonstrate how the current-induced spin torque distorts moving DW with respect to the equilibrium Néel configuration by generating a nonzero $M_i^y \neq 0$ component.

Since TDNEGF also captures transient charge and spin currents after the dc bias voltage is turned on at $t = 0$, we first evolve the conduction electron subsystem (during $t < 1$ ps in Fig. 3) with fixed DW (i.e., without coupling to the LLG equations) until such currents become steady. This evolution ensures that at $t = 1$ ps, when LLG dynamics is turned on, the spatial profiles of $\mathbf{S}_{\text{CD}}^i(t)$ computed by TDNEGF and NEGF formalisms are identical. The position of the DW center as a function of time in Fig. 4 computed by TDNEGF+LLG is similar to the LLG result obtained in Fig. 1 of Ref. [21]. On the other hand, it differs from the LLG results of Refs. [35,36] and related NEGF+LLG results of Ref. [48], where X_{DW} becomes saturated after a relatively short time (i.e., DW motion comes quickly to a halt) for $E_F < J_{sd}$, while DW continues to move for $E_F > J_{sd}$ with X_{DW} exhibiting high-frequency oscillations (i.e., regularly accelerating and slowing down the DW) due to the excitation of the spin waves [36,48]. This discrepancy could be due to the time-retarded damping [63,64] present in TDNEGF+LLG but absent in the NEGF+LLG framework, which can strongly affect [65] spin-wave excitation.

Most importantly, the TDNEGF+LLG framework predicts faster DW motion in Fig. 4 when compared to the



VIDEO 1. Animation of $\mathbf{M}_i(t)$ from Fig. 3 and $X_{\text{DW}}(t)$ from 4 for DW motion driven by steady current due to dc bias voltage. We use $E_F^b = 0.05$ eV $<$ $J_{sd} = 0.1$ eV in this animation.

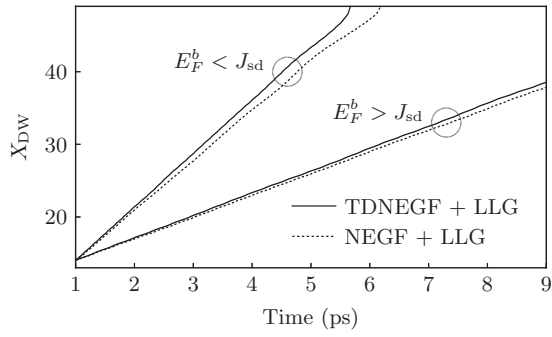


FIG. 4. The position X_{DW} of the DW center as a function of time for $E_F^b = 0.05$ eV $< J_{sd} = 0.1$ eV and $E_F^b = 0.15$ eV $> J_{sd} = 0.1$ eV computed using TDNEGF+LLG (solid lines) and NEGF + LLG (dashed lines) formalisms applied to the device in Fig. 1 with dc bias voltage $eV_b = 0.05$ eV.

NEGF + LLG results. This prediction can be explained by the additional torque exerted onto the DW by the pumped [58,59] spin currents of electrons in the presence of localized magnetic-moment precession, as depicted in Video 1, which is a purely time-dependent quantum-mechanical effect absent in either LLG or NEGF+LLG simulations. Although the difference between the TDNEGF+LLG and NEGF+LLG results in Fig. 4 is small over the time interval considered, a much larger one can be extrapolated as one approaches ~ 10 ns typical time of DW motion in experiments and applications [67–71].

The TDNEGF+LLG framework allows us to obtain explicitly the time-dependent charge I_p [Figs. 5(a)

and 5(c)] and spin $I_p^{S_\alpha}$ [Figs. 5(d), 5(g), 5(j), 5(f), 5(i), and 5(l)] currents flowing into the NM leads in the course of DW motion, as well as the spatiotemporal profiles of local charge $I_{i \rightarrow j}$ [Fig. 5(b)] and local spin $I_{i \rightarrow j}^{S_\alpha}$ [Figs. 5(e), 5(h), and 5(k)] currents flowing between the nearest-neighbor sites. Note that these time-dependent currents are superimposed on the background of injected dc charge current or dc spin current generated by the spin-polarizing effect of the localized magnetic moments on the injected dc current (the background values can be read from the flat lines within the $t < 1$ ps interval in Fig. 5).

Since Video 1 of the time evolution of $\mathbf{M}_i(t)$ shows that three localized magnetic moments around the propagating DW center are precessing, to gain intuition about how they induce spin and charge pumping in Fig. 5, we first examine the simplest example of a single [Figs. 6(a)–6(c)] or up to five [Fig. 6(d)] magnetic moments $\mathbf{M}_i(t)$ precessing steadily with frequency ω and precession cone angle θ while being coupled to an infinite 1D TB chain [59]. This setup—precessing spins in the center of a 1D TB chain (for an illustration, see Fig. 1 in Ref. [59])—pumps only spin currents in both directions, as shown in Fig. 6(b). This problem is exactly solvable in the rotating frame, where our result in Fig. 6(b), after transient currents in Fig. 6(a) die away, matches the analytical formula derived in Ref. [59], thereby also validating the accuracy of TDNEGF numerical calculations. In particular, time-independent $I_p^{S_z}$ in Fig. 6(c) exhibits standard $\propto \sin^2 \theta$ dependence [58] on the precession cone angle θ . The maximum output in Fig. 6(d) is achieved by using three magnetic moments

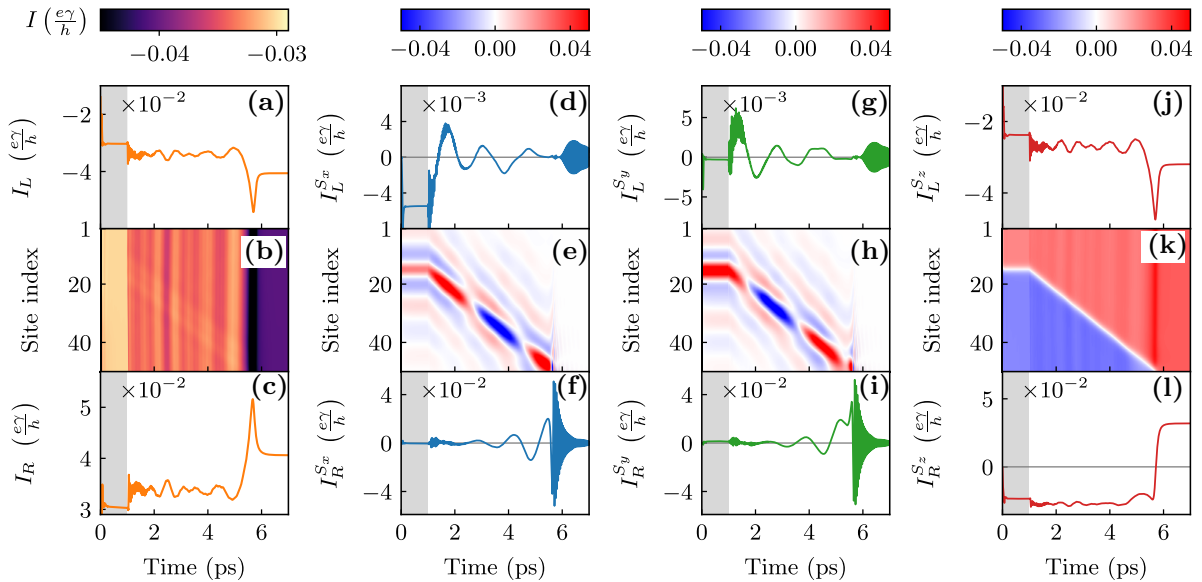


FIG. 5. Charge current in the (a) left and (c) right NM leads, as well as spin currents in the (d),(g),(j) left and (f),(i),(l) right NM leads. These currents are steady (after transient time following the switching of dc bias voltage at $t = 0$) in the shaded area (for $t < 1$ ps), where DW is fixed at $X_{\text{DW}} = 15$, but they become time dependent after coupling to LLG dynamics is turned on for $t \geq 1$ ps. Panels (b) and (e),(h),(k) depict the spatiotemporal profile of the local (bond) charge and spin currents, respectively. The parameters are chosen as $E_F^b = 0.05$ eV, $J_{sd} = 0.1$ eV, and $eV_b = 0.05$ eV.

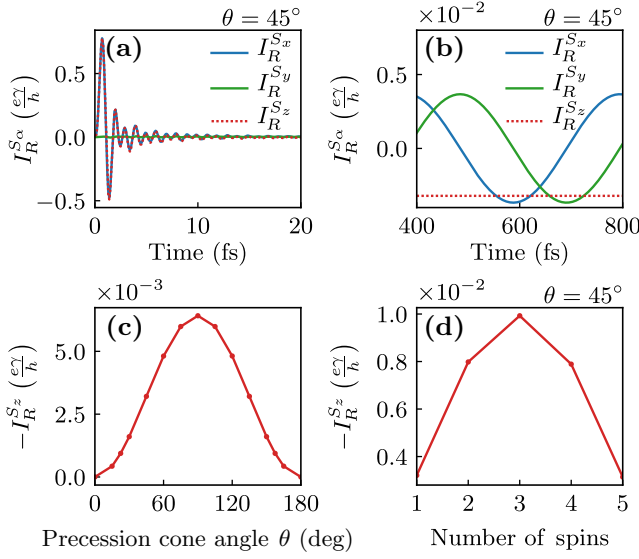


FIG. 6. (a),(b) Time dependence of spin currents $I_R^{S\alpha}(t)$ in the right lead of an infinite TB chain hosting a single magnetic moment in the middle, precessing steadily with frequency $\hbar\omega = 1 \times 10^{-2}$ eV and cone angle $\theta = 45^\circ$ in the absence of any dc bias voltage (for an illustration of this setup, see Fig. 1 in Ref. [59]). Spin currents in the left lead have the same magnitude, but opposite direction. (c) I_R^z , which is steady in panel (b), as a function of precession cone angle θ . (d) Scaling of I_R^z with the number of precessing magnetic moments. The parameters are chosen as $E_F^b = 2$ eV and $J_{sd} = 1$ eV, as well as $J \equiv 0$ in the case of more than one precessing magnetic moment in panel (d).

precessing together, which signifies the interfacial nature [58,59] of spin pumping.

In addition, even a single precessing magnetic moment can pump a charge current with a nonzero dc component with the proviso that the key requirement in the theory of quantum charge pumping by a time-dependent field is satisfied [84–87]—breaking of left-right symmetry. This condition requires us to break the inversion symmetry and/or time-reversal symmetry. If both the inversion and time-reversal symmetries are broken dynamically, the dc component of pumped charge current is $\propto \Omega$ at low frequencies, as found in the standard example of a quantum dot attached to two leads and exposed to two spatially separated potentials oscillating out of phase [84,85]. If only one of those two symmetries is broken, and this does not have to occur dynamically, the dc component of the pumped current is $\propto \Omega^2$ at low frequencies. For example, this is found when a static potential barrier is introduced to break the inversion symmetry into 1D TB chain hosting a single precessing magnetic moment [59].

Armed with this intuition, we can interpret currents in Figs. 5(b), 5(e), 5(h), and 5(k) as the consequence of moving the DW center pumping spin and charge currents due to the dynamics of magnetic moments around the DW center depicted in Video 1. The pumped charge current

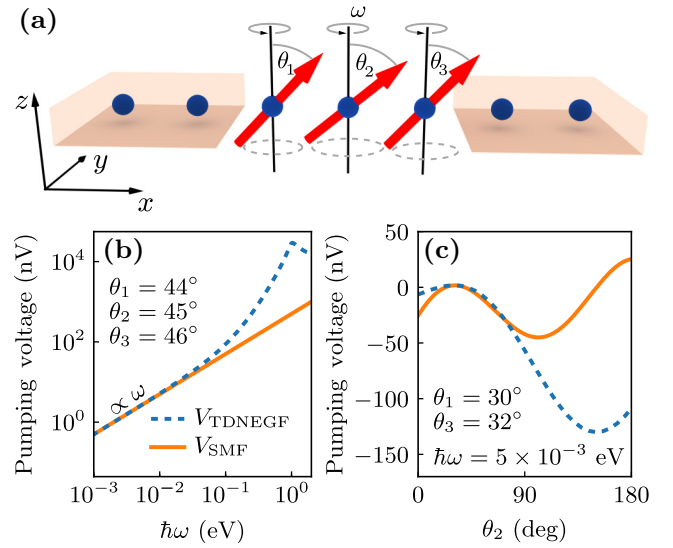


FIG. 7. (a) Schematic view of a toy noncollinear and noncoplanar system, consisting of three localized magnetic moments in the middle of an infinite TB chain precessing at the same frequency ω but with different cone angles, which pumps spin and charge current into the semi-infinite leads in the absence of any bias voltage ($V_b \equiv 0$). The magnetic moments do not interact with each other ($J \equiv 0$). Their s - d interaction with electrons within the TB chain is $J_{sd} = 0.1$ eV and electronic Fermi energy is chosen as $E_F^b = 3.0$ eV. (b) The dc pumping voltage between the leads as a function of ω for small noncollinearity of magnetic moments, $\theta_1 = 44^\circ$, $\theta_2 = 45^\circ$ and $\theta_3 = 46^\circ$. (c) The dc pumping voltage between the leads as a function of θ_2 while $\theta_1 = 30^\circ$ and $\theta_3 = 32^\circ$ are fixed and all three localized magnetic moments are precessing at a fixed frequency $\hbar\omega = 5 \times 10^{-3}$ eV. The voltages in panels (b) and (c) are computed either from Eqs. (15) and (16) of the SMF theory [77,78] (solid line) or numerically exactly from the TDNEGF formalism (dashed line).

arises because the DW itself breaks the left-right symmetry, while the localized magnetic moments around its center are driven into precession by spin torque, as visualized in Fig. 3. The collision of the DW with the right NM lead results in its annihilation; i.e., all \mathbf{M}_i eventually point along the z axis, which generates a spike in the charge and spin currents in Fig. 5 around $t \simeq 6$ ps.

While a variety of techniques have been developed to determine the position of a moving DW [6,88,89], they often have limitations in resolution or acquisition speed [89]. Figure 5 shows that temporal profiles of $I_p^{Sx}(t)$ and $I_p^{Sy}(t)$ are tightly correlated with the DW position and that their amplitude increases (decreases) as the DW approaches (recedes from) the NM lead. Thus, converting these spin currents into ac voltage via the inverse spin Hall effect, which can be done experimentally with high efficiency [90], offers an electrical measurement that precisely tracks the position of a single DW propagating along magnetic nanowire.

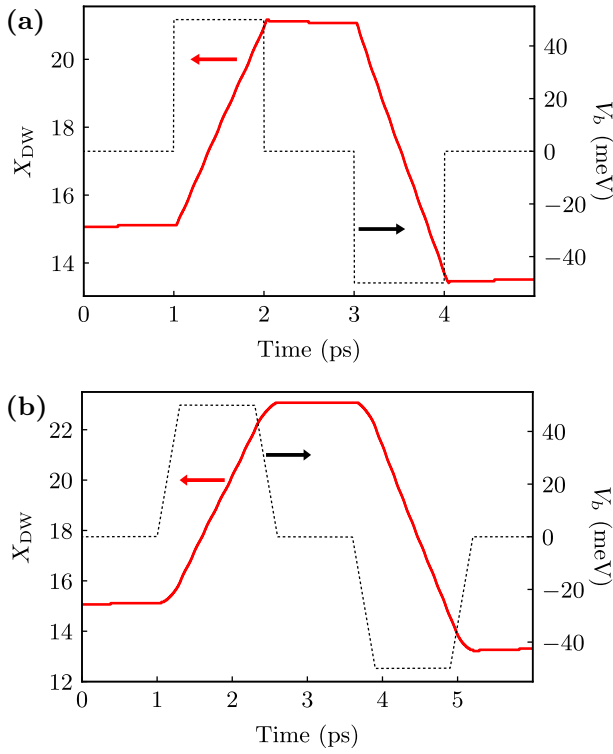


FIG. 8. The position X_{DW} of the DW center as a function of time, where the DW motion is induced by applying (a) a sequence of two successive rectangular voltage pulses or (b) a sequence of two successive trapezoidal voltage pulses. The temporal characteristics of the sequence of two pulses of opposite polarity are depicted by the dashed line, while their magnitude $|eV_b^{\text{max}}| = 0.05$ eV is the same as the dc bias voltage employed in Figs. 3, 4, and 5. The parameters are chosen as $E_F^b = 0.05$ eV and $J_{sd} = 0.1$ eV.

IV. TDNEGF+LLG VS. SPIN-MOTIVE FORCE THEORY FOR CHARGE CURRENT PUMPED BY TIME-DEPENDENT MAGNETIC TEXTURES

The spin-motive force (SMF) [62,77,78,91–100] refers to pumping of charge and spin currents, or generation of voltage associated with pumped charge current, by time-dependent noncoplanar and noncollinear magnetic textures within conducting ferromagnets. In contrast to conventional electromotive force induced by the change of magnetic flux through a circuit in accord with the Faraday law of classical electromagnetism, SMF originates from spin and can appear even in a static uniform external magnetic field (as long as such a field generates dynamics of the localized magnetic moments). The SMF has been invoked to explain the experimental detection of electric voltage due to the motion of magnetic DW [101], the magnetization reversal of nanoparticles embedded in a MTJ [102], and the gyration of the magnetic vortex core [103]. Since the SMF phenomenon is certainly related to the charge

current pumping explored in Sec. III, here, we investigate this relationship in detail.

The voltage associated with the SMF between the edges of the wire lying along the x axis [77]

$$V_{\text{SMF}} = \frac{1}{\sigma_0} \int j_x dx, \quad (15)$$

is obtained from the pumped local charge current [78]

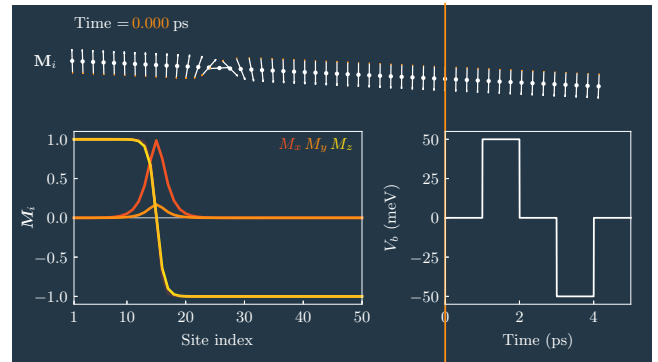
$$j_\alpha(\mathbf{r}) = \frac{P\sigma_0\hbar}{2e} [\partial_t \mathbf{m}(\mathbf{r}, t) \times \partial_\alpha \mathbf{m}(\mathbf{r}, t)] \cdot \mathbf{m}(\mathbf{r}, t), \quad (16)$$

where $\partial_t = \partial/\partial t$ and $\partial_\alpha = \partial/\partial \alpha$ for $\alpha \in \{x, y, z\}$; $\sigma_0 = \sigma^\uparrow + \sigma^\downarrow$ is the total conductivity; and $P = (\sigma^\uparrow - \sigma^\downarrow)/(\sigma^\uparrow + \sigma^\downarrow)$ is the spin polarization of the ferromagnet. In general, conductivities σ^\uparrow and σ^\downarrow for the spin- \uparrow and spin- \downarrow bands depend on the external magnetic field due to the magnetoresistive effect, but this dependence can be neglected for transition metal ferromagnets. Similarly, part of the 3×3 tensor of a pumped local spin current flowing along the α axis is given by the vector [78]

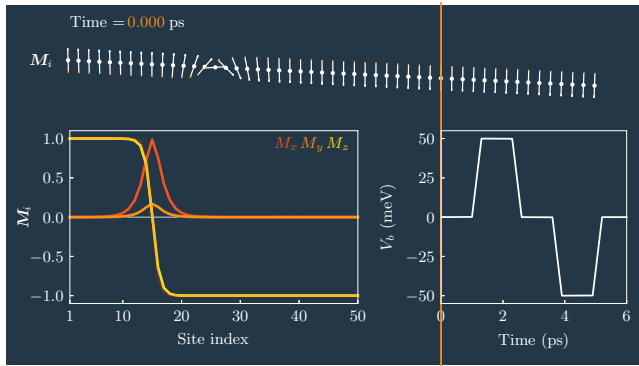
$$[j_\alpha^{S_x}(\mathbf{r}), j_\alpha^{S_y}(\mathbf{r}), j_\alpha^{S_z}(\mathbf{r})] = \frac{g\mu_B\hbar\sigma_0}{4e^2} [\partial_t \mathbf{m}(\mathbf{r}, t) \times \partial_\alpha \mathbf{m}(\mathbf{r}, t)], \quad (17)$$

where μ_B is the Bohr magneton.

Equations (16) and (17) contain only the lowest-order time and spatial derivatives of magnetization [104], so that comparing them to our nonperturbative results from TDNEGF+LLG makes it possible to establish limits of validity of these equations. For this purpose, we employ a toy noncoplanar and noncollinear system consisting of three localized magnetic moments precessing with the same frequency ω , which is illustrated in Fig. 7(a), and it is akin to the system analyzed in Fig. 6(d) but with different precession cone angles θ_1 , θ_2 , and θ_3 . Similarly to studies combining classical micromagnetics with the SMF formula [105], the temporal dependence of these three



VIDEO 2. Animation of $X_{\text{DW}}(t)$ from Fig. 8(a) and $\mathbf{M}_i(t)$ for DW motion driven by a sequence of two successive rectangular voltage pulses.



VIDEO 3. Animation of $X_{\text{DW}}(t)$ from Fig. 8(b) and $\mathbf{M}_i(t)$ for DW motion driven by a sequence of two successive trapezoidal voltage pulses.

localized magnetic moments is plugged into the discretized version of Eq. (16):

$$\begin{aligned} j_x(i) &\propto \frac{1}{a} [\partial_t \mathbf{M}_i(t) \times (\mathbf{M}_{i+1}(t) - \mathbf{M}_i(t))] \cdot \mathbf{M}_i(t) \\ &\propto \frac{1}{a} [\partial_t \mathbf{M}_i(t) \times \mathbf{M}_{i+1}(t)] \cdot \mathbf{M}_i(t). \end{aligned} \quad (18)$$

Since Eqs. (15) and (18) do not allow us to compute charge current flowing into the leads, we plug $j_x(i)$ from Eq. (18) into Eq. (15) to obtain the SMF voltage V_{SMF} between the edges of the central region in Fig. 7(a). This voltage is then compared to the pumping voltage $V_{\text{TDNEGF}} = I_p/G$ in an open circuit computed using the charge current I_p in Eq. (11) pumped into NM leads and the two-terminal conductance G obtained from the Landauer formula.

For small noncollinearity between three magnetic moments in Fig. 7(a) ($\theta_1 = 44^\circ$, $\theta_2 = 45^\circ$, and $\theta_3 = 46^\circ$) voltages V_{SMF} and V_{TDNEGF} track each other in Fig. 7(b), while following $\propto \omega$ dependence. This perfect tracking is satisfied for all frequencies relevant for magnetization dynamics, where the highest is in the THz range (or $\hbar\omega \sim 0.004$ eV) as encountered in the dynamics of antiferromagnets [106]. However, if we fix the precession frequency and change angles between neighboring magnetic moments, we find increasing deviation between V_{SMF} and V_{TDNEGF} once the relative angles become $\gtrsim 10^\circ$ in Fig. 7(c), which can reach a factor-of-2 difference at large angles.

V. DW MOTION DRIVEN BY PULSE CURRENT: TRANSIENT INERTIAL DISPLACEMENT AND SPIN AND CHARGE PUMPING

The pulse-current-driven DW motion is of particular relevance for racetrack memory applications [17,18], where digital information is characterized by the orientation of the magnetic domain and data processing is carried out via current-induced DW motion. Thus, precise control of

the position of the DW is required to achieve successful memory operation [38,69–71]. Although the DW displacement is related to the current pulse duration, it is in general not a linear relation due to the transient inertial displacement (or automotion) [38,69,71,72,107] appearing at the current pulse onset and after pulse termination. Thus, a too-large transient inertial displacement will be detrimental for racetrack memory operation. The origin of transient inertial displacement is deformation of the DW leading to a delayed response at the current onset and at the end of the current pulse, which then requires us to tune the duration [38,69–71] and the shape (i.e., its rise and fall time) [72] of the pulse. The experiments [69–71] and classical micromagnetic simulations [38,70,72] typically employ short, ns pulses, which generate higher DW velocities than longer, μs pulses due to easier depinning by an additional force on the DW during the pulse rise time or by a small mean distance between the pinning centers.

We apply a sequence of two successive voltage pulses of opposite polarity whose temporal characteristics are shown in Fig. 8 and whose magnitude is the same as the dc bias voltage used in Figs. 3, 4, and 5. We use rectangular [Fig. 8(a)] or trapezoidal [Fig. 8(b)] pulses of ps duration to understand the basic physics and reduce the computational expense. The first pulse drives the DW forward (i.e., in the positive x direction in Fig. 1) and the second pulse drives the DW backward, as illustrated by Videos 2 and 3, corresponding to Figs. 8(a) and 8(b), respectively. Thus, in the absence of transient inertial displacement, the DW center should return to its initial position in Fig. 8. The transient inertial displacement in Fig. 8, $\delta X_{\text{DW}} = X_{\text{DW}}(t=0) - X_{\text{DW}}(t=5\text{ps})$, is approximately 10% of the forward displacement generated by the first pulse and surprisingly close to the transient displacement observed in experiments where adiabatic spin torque drives the DW motion [71]. On the other hand, it is quite different from the transient inertial displacement estimated [38] via a simple formula, $\delta X_{\text{DW}} = -W\delta\phi/\lambda$, using a 1D model of the DW ($\delta\phi$ is the angle variation of the DW, which is $\delta\phi = \pi$ in the case of the DW in Fig. 1). Thus, $\delta X_{\text{DW}} \sim 10\text{--}100$ nm predicted by this formula, for the typical Gilbert damping $\lambda \sim 0.01\text{--}0.1$ of magnetic nanowires, suggests a transient displacement comparable to or much larger than the bit size of the racetrack memory (~ 10 nm bit size is required for racetrack memory to be competitive with other memory devices [17,18]), which would be a significant impediment for its operation. Since it contradicts experiments where a much smaller δX_{DW} has been observed [71], researchers aiming to reproduce such an observation with classical micromagnetic simulations have suggested [71] that the engineering of extrinsic pinning sites is necessary to obtain small δX_{DW} .

Conversely, the small δX_{DW} that we obtain in Fig. 8 for perfectly clean nanowires suggests the importance of the inclusion of time-dependent quantum transport effects,

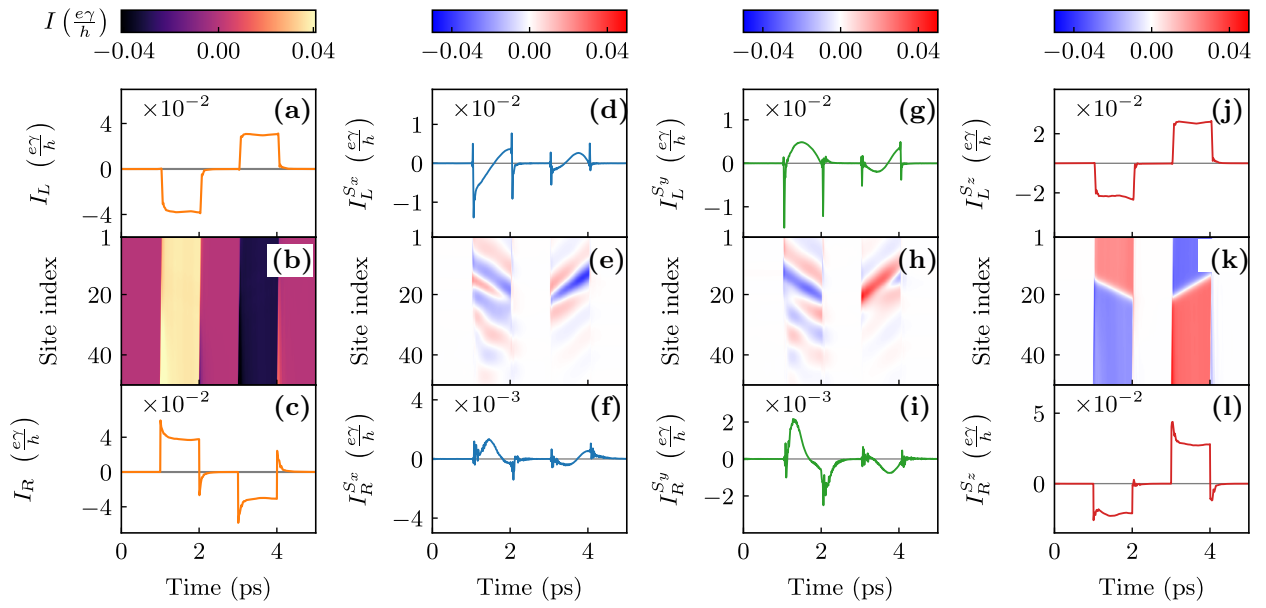


FIG. 9. Time dependence of charge current in the (a) left and (c) right NM leads, as well as spin currents in the (d),(g),(j) left and (f),(i),(l) right NM leads in the course of DW motion induced by a sequence of two successive rectangular voltage pulses depicted in Fig. 8(a). Panels (b) and (e),(h),(k) depict the spatiotemporal profile of the local (bond) charge and spin currents, respectively. The parameters are chosen as $E_F^b = 0.05$ eV, $J_{sd} = 0.1$ eV.

such as the spin and charge pumping generated while the DW experiences acceleration and deceleration due to the injected pulse current, as well as the time-retarded damping introduced by the TDNEGF into the LLG equation [in addition to the intrinsic Gilbert damping term in Eq. (7)]. Figure 9 shows the spin and charge currents in the NM leads, as well as locally between the sites of the magnetic nanowire, which emerge upon applying a sequence of the two rectangular pulses depicted in Fig. 9(a) and can be contrasted to the same information presented in Fig. 5 for the case of applied dc charge current. The charge currents in Figs. 9(a) and 9(c) do not follow the shape of the pulse due to the additional charge current being pumped when the DW starts or stops moving. The same applies to the $I_p^{S_z}$ spin current, which, in the absence of DW motion, would quantify the spin polarization $I_p^{S_z}/I$ [108] along the z axis after the injected unpolarized charge current becomes polarized via propagation through the magnetic nanowire depicted in Fig. 1. The spikes in spin currents at the instants of time where the pulse rises or decays introduce additional terms in the LLG dynamics that are absent in classical micromagnetics.

VI. CONCLUSIONS

In conclusion, we develop a multiscale theoretical and computational framework that self-consistently couples a time-dependent nonequilibrium quantum statistical description of conduction electrons with a time-dependent classical description of localized magnetic moments. The TDNEGF+LLG framework requires just time-dependent

quantum and classical Hamiltonians, together with device geometry, as an input for computing the time evolution of the interacting electron-localized-magnetic-moments many-body system in a numerically exact fashion. This method can be contrasted with widely used classical micromagnetic simulations [2,3,7,8,20,21,21,35–43,71], where propagating conduction electrons appear only indirectly through phenomenological spin-torque terms inserted by hand into the LLG equation or with previous steady-state-NEGF+LLG attempts [48–52] to couple quantum electrons to classical localized magnetic moments, where fast electrons are assumed to instantaneously respond to slow dynamics of localized magnetic moments so that noncommutativity of the electronic quantum Hamiltonian at different times is neglected. Using DW motion, driven by steady or pulse-injected charge current as an example, we essentially demonstrate the introduction (via TDNEGF) of quantum spin pumping by the dynamics of localized magnetic moments and additional time-retarded damping characterized by a memory kernel [63,64] into classical micromagnetics. In addition, we nonperturbatively quantify the charge and spin currents pumped from a time-dependent magnetic texture into the attached NM leads. They can be used as signatures of the dynamics of DWs, skyrmions, and spin superfluids [109] that can be detected by standard charge transport measurements. The same problem of charge pumping by time-dependent magnetic textures is also tackled by the SMF theory [62,77,78,91–100,105]. However, its analytical formula in Eq. (16) is perturbative in nature (i.e., it contains only the lowest-order time and spatial

derivatives of magnetization) and direct comparison with the nonperturbative TDNEGF+LLG framework shows [Fig. 7] that it fails when angles between neighboring localized magnetic moments exceed approximately 10° .

ACKNOWLEDGMENTS

We thank L.E.F. Foa Torres for instructive discussions. M.D.P. and P.P. are supported by ARO MURI Grant No. W911NF-14-0247. B.S.P., U.B., and B.K.N. are supported by NSF Grant No. CHE 1566074. The supercomputing time is provided by XSEDE, which is supported by NSF Grant No. ACI-1548562.

-
- [1] D. Ralph and M. Stiles, Spin transfer torques, *J. Magn. Mater.* **320**, 1190 (2008).
- [2] J. Xiao, A. Zangwill, and M. D. Stiles, Macrospin models of spin transfer dynamics, *Phys. Rev. B* **72**, 014446 (2005).
- [3] D. V. Berkov and J. Miltat, Spin-torque driven magnetization dynamics: Micromagnetic modeling, *J. Magn. Mater.* **320**, 1238 (2008).
- [4] A. Yamaguchi, T. Ono, S. Nasu, K. Miyake, K. Mibu, and T. Shinjo, Real-Space Observation of Current-Driven Domain Wall Motion in Submicron Magnetic Wires, *Phys. Rev. Lett.* **92**, 077205 (2004).
- [5] G. Tatara, H. Kohno, and J. Shibata, Microscopic approach to current-driven domain wall dynamics, *Phys. Rep.* **468**, 213 (2008).
- [6] K.-J. Kim, Y. Yoshimura, and T. Ono, Current-driven magnetic domain wall motion and its real-time detection, *Jap. J. Appl. Phys.* **56**, 0802A4 (2017).
- [7] K.-J. Lee, A. Deac, O. Redon, J.-P. Nozières, and B. Dieny, Excitations of incoherent spin-waves due to spin-transfer torque, *Nat. Mater.* **3**, 877 (2004).
- [8] M. Baumgartner *et al.*, Spatially and time-resolved magnetization dynamics driven by spin-orbit torques, *Nat. Nanotech.* **12**, 980 (2017).
- [9] N. Nagaosa and Y. Tokura, Topological properties and dynamics of magnetic skyrmions, *Nat. Nanotech.* **8**, 899 (2013).
- [10] A. Fert, V. Cros, and J. Sampaio, Skyrmions on the track, *Nat. Nanotech.* **8**, 152 (2013).
- [11] N. Locatelli, V. Cros, and J. Grollier, Spin-torque building blocks, *Nat. Mater.* **13**, 11 (2014).
- [12] A. D. Kent and D. C. Worledge, A new spin on magnetic memories, *Nat. Nanotech.* **10**, 187 (2015).
- [13] J. Grollier, D. Querlioz, and M. D. Stiles, Spintronic nanodevices for bioinspired computing, *Proc. IEEE* **104**, 2024 (2016).
- [14] W. A. Borders, H. Akima, S. Fukami, S. Moriya, S. Kurihara, Y. Horio, S. Sato, and H. Ohno, Analogue spinorbit torque device for artificial-neural-network-based associative memory operation, *Appl. Phys. Expr.* **10**, 013007 (2017).
- [15] A. Manchon, I. M. Miron, T. Jungwirth, J. Sinova, J. Zelezny, A. Thiaville, K. Garello, and P. Gambardella, Current-induced spin-orbit torques in ferromagnetic and antiferromagnetic systems, [arXiv.org/abs/1801.09636](https://arxiv.org/abs/1801.09636).
- [16] B. K. Nikolić, K. Dolui, M. Petrović, P. Plecháč, T. Markussen, and K. Stokbro, First-principles quantum transport modeling of spin-transfer and spin-orbit torques in magnetic multilayers, in W. Andreoni and S. Yip (eds.) *Handbook of Materials Modeling* (Springer, Cham, 2018); [arXiv.org/abs/1801.05793](https://arxiv.org/abs/1801.05793).
- [17] S. S. P. Parkin, M. Hayashi, and L. Thomas, Magnetic domain-wall racetrack memory, *Science* **320**, 190 (2008).
- [18] S. Parkin and S.-H. Yang, Memory on the racetrack, *Nat. Nanotech.* **10**, 195 (2015).
- [19] W. Koshibae, Y. Kaneko, J. Iwasaki, M. Kawasaki, Y. Tokura, and N. Nagaosa, Memory functions of magnetic skyrmions, *Jap. J. Appl. Phys.* **54**, 053001 (2015).
- [20] R. F. L. Evans, W. J. Fan, P. Chureemart, T. A. Ostler, M. O. A. Ellis, and R. W. Chantrell, Atomistic spin model simulations of magnetic nanomaterials, *J. Phys.: Condens. Matter* **26**, 103202 (2014).
- [21] M. D. Stiles, W. M. Saslow, M. J. Donahue, and A. Zangwill, Adiabatic domain wall motion and Landau-Lifshitz damping, *Phys. Rev. B* **75**, 214423 (2007); N. Smith, Comment on “Adiabatic domain wall motion and Landau-Lifshitz damping”, *Phys. Rev. B* **78**, 216401 (2008).
- [22] P. M. Haney, D. Waldron, R. A. Duine, A. S. Núñez, H. Guo, and A. H. MacDonald, Current-induced order parameter dynamics: Microscopic theory applied to Co/Cu/Co spin valves, *Phys. Rev. B* **76**, 024404 (2007).
- [23] S. Wang, Y. Xu, and K. Xia, First-principles study of spin-transfer torques in layered systems with noncollinear magnetization, *Phys. Rev. B* **77**, 184430 (2008).
- [24] Z. Yu, L. Zhang, and J. Wang, First-principles investigation of transient spin transfer torque in magnetic multilayer systems, *Phys. Rev. B* **96**, 075412 (2017).
- [25] I. Theodonis, N. Kioussis, A. Kalitsov, M. Chshiev, and W. H. Butler, Anomalous Bias Dependence of Spin Torque in Magnetic Tunnel Junctions, *Phys. Rev. Lett.* **97**, 237205 (2006).
- [26] C. Heiliger and M. D. Stiles, *Ab Initio* Studies of the Spin-Transfer Torque in Magnetic Tunnel Junctions, *Phys. Rev. Lett.* **100**, 186805 (2008).
- [27] M. Stamenova, R. Mohebbi, J. Seyed-Yazdi, I. Rungger, and S. Sanvito, First-principles spin-transfer torque in CuMnAs—GaP—CuMnAs junctions, *Phys. Rev. B* **95**, 060403 (2017).
- [28] S. Zhang and Z. Li, Roles of Nonequilibrium Conduction Electrons on the Magnetization Dynamics of Ferromagnets, *Phys. Rev. Lett.* **93**, 127204(R) (2004).
- [29] I. Garate, K. Gilmore, M. D. Stiles, and A. H. MacDonald, Nonadiabatic spin-transfer torque in real materials, *Phys. Rev. B* **79**, 104416 (2009).
- [30] P. Baláž, V. K. Dugaev, and J. Barnaś, Spin-transfer torque in a thick Néel domain wall, *Phys. Rev. B* **85**, 024416 (2012).
- [31] X. Waintal and M. Viret, Current-induced distortion of a magnetic domain wall, *EPL* **65**, 427 (2004).
- [32] J. Xiao, A. Zangwill, and M. D. Stiles, Spin-transfer torque for continuously variable magnetization, *Phys. Rev. B* **73**, 054428 (2006).

- [33] G. Tatara, H. Kohno, J. Shibata, Y. Lemaho, and K.-J. Lee, Spin torque and force due to current for general spin textures, *J. Phys. Soc. Japan* **76**, 054707 (2007).
- [34] Z. Yuan and P. J. Kelly, Spin-orbit-coupling induced torque in ballistic domain walls: Equivalence of charge-pumping and nonequilibrium magnetization formalisms, *Phys. Rev. B* **93**, 224415 (2016).
- [35] Z. Li and S. Zhang, Domain-wall dynamics driven by adiabatic spin-transfer torques, *Phys. Rev. B* **70**, 024417 (2004).
- [36] Z. Li and S. Zhang, Domain-Wall Dynamics and Spin-Wave Excitations with Spin-Transfer Torques, *Phys. Rev. Lett.* **92**, 207203 (2004).
- [37] A. Thiaville, Y. Nakatani, J. Miltat, and Y. Suzuki, Micromagnetic understanding of current-driven domain wall motion in patterned nanowires, *EPL* **69**, 990 (2005).
- [38] A. Thiaville, Y. Nakatani, F. Piéchon, J. Miltat, and T. Ono, Transient domain wall displacement under spin-polarized current pulses, *Eur. Phys. J. B* **60**, 15 (2007).
- [39] E. Martinez, L. Lopez-Diaz, O. Alejos, L. Torres, and M. Carpentieri, Domain-wall dynamics driven by short pulses along thin ferromagnetic strips: Micromagnetic simulations and analytical description, *Phys. Rev. B* **79**, 094430 (2009).
- [40] C. T. Boone and I. N. Krivorotov, Magnetic Domain Wall Pumping by Spin Transfer Torque, *Phys. Rev. Lett.* **104**, 167205 (2010).
- [41] P. Chureemart, R. F. L. Evans, and R. W. Chantrell, Dynamics of domain wall driven by spin-transfer torque, *Phys. Rev. B* **83**, 184416 (2011).
- [42] J. Iwasaki, M. Mochizuki, and N. Nagaosa, Current-induced skyrmion dynamics in constricted geometries, *Nat. Nanotech.* **8**, 742 (2013).
- [43] J. Sampaio, V. Cros, S. Rohart, A. Thiaville, and A. Fert, Nucleation, stability and current-induced motion of isolated magnetic skyrmions in nanostructure, *Nat. Nanotech.* **8**, 839 (2013).
- [44] M. E. Knoester, J. Sinova, and R. A. Duine, Phenomenology of current-skyrmion interactions in thin films with perpendicular magnetic anisotropy, *Phys. Rev. B* **89**, 064425 (2014).
- [45] K. M. D. Hals and A. Brataas, Spin-orbit torques and anisotropic magnetization damping in skyrmion crystals, *Phys. Rev. B* **89**, 064426 (2014).
- [46] H.-B. Braun, Topological effects in nanomagnetism: From superparamagnetism to chiral quantum solitons, *Adv. Phys.* **61**, 1 (2012).
- [47] C. A. Akosa, P. B. Ndiaye, and A. Manchon, Intrinsic nonadiabatic topological torque in magnetic skyrmions and vortices, *Phys. Rev. B* **95**, 054434 (2017).
- [48] J. I. Ohe and B. Kramer, Dynamics of a Domain Wall and Spin-Wave Excitations Driven by a Mesoscopic Current, *Phys. Rev. Lett.* **96**, 027204 (2006).
- [49] J. I. Ohe and B. Kramer, Current-induced spin fluctuation state in a mesoscopic magnetic wire, *Phys. Rev. B* **74**, 201305(R) (2006).
- [50] S. Salahuddin and S. Datta, Self-consistent simulation of quantum transport and magnetization dynamics in spin-torque based devices, *Appl. Phys. Lett.* **89**, 153504 (2006).
- [51] M. O. A. Ellis, M. Stamenova, and S. Sanvito, Multiscale modeling of current-induced switching in magnetic tunnel junctions using *ab initio* spin-transfer torques, *Phys. Rev. B* **96**, 224410 (2017).
- [52] Y. Xie, J. Ma, S. Ganguly, and A. W. Ghosh, From materials to systems: A multiscale analysis of nanomagnetic switching, *J. Comput. Electron.* **16**, 1201 (2017).
- [53] C. A. Akosa, W.-S. Kim, A. Bisig, M. Kläui, K.-J. Lee, and A. Manchon, Role of spin diffusion in current-induced domain wall motion for disordered ferromagnets, *Phys. Rev. B* **91**, 094411 (2015).
- [54] D. Claudio-Gonzalez, A. Thiaville, and J. Miltat, Domain Wall Dynamics Under Nonlocal Spin-Transfer Torque, *Phys. Rev. Lett.* **108**, 227208 (2012).
- [55] K.-J. Lee, M. D. Stiles, H.-W. Lee, J.-H. Moon, K.-W. Kim, and S.-W. Lee, Self-consistent calculation of spin transport and magnetization dynamics, *Phys. Rep.* **531**, 89 (2013).
- [56] M. Sturma, C. Bellegarde, J.-C. Toussaint, and D. Gusakova, Simultaneous resolution of the micromagnetic and spin transport equations applied to current-induced domain wall dynamics, *Phys. Rev. B* **94**, 104405 (2016).
- [57] G. Stefanucci and R. van Leeuwen, *Nonequilibrium Many-Body Theory of Quantum Systems: A Modern Introduction* (Cambridge University Press, Cambridge, 2013).
- [58] Y. Tserkovnyak, A. Brataas, G. E. W. Bauer, and B. I. Halperin, Nonlocal magnetization dynamics in ferromagnetic heterostructures, *Rev. Mod. Phys.* **77**, 1375 (2005).
- [59] S.-H. Chen, C.-R. Chang, J. Q. Xiao, and B. K. Nikolić, Spin and charge pumping in magnetic tunnel junctions with precessing magnetization: A nonequilibrium Green function approach, *Phys. Rev. B* **79**, 054424 (2009).
- [60] K. M. D. Hals, A. Brataas, and Y. Tserkovnyak, Scattering theory of charge-current induced magnetization dynamics, *EPL* **90**, 47002 (2010).
- [61] F. Mahfouzi, J. Fabian, N. Nagaosa, and B. K. Nikolić, Charge pumping by magnetization dynamics in magnetic and semimagnetic tunnel junctions with interfacial Rashba or bulk extrinsic spin-orbit coupling, *Phys. Rev. B* **85**, 054406 (2012).
- [62] K.-W. Kim, J.-H. Moon, K.-J. Lee, and H.-W. Lee, Prediction of Giant Spin Motive Force due to Rashba Spin-Orbit Coupling, *Phys. Rev. Lett.* **108**, 217202 (2012).
- [63] M. Sayad and M. Potthoff, Spin dynamics and relaxation in the classical-spin Kondo-impurity model beyond the Landau-Lifshitz-Gilbert equation, *New J. Phys.* **17**, 113058 (2015).
- [64] H. Hammar and J. Fransson, Time-dependent spin and transport properties of a single-molecule magnet in a tunnel junction, *Phys. Rev. B* **94**, 054311 (2016).
- [65] T. Bose and S. Trimper, Retardation effects in the Landau-Lifshitz-Gilbert equation, *Phys. Rev. B* **83**, 134434 (2011).
- [66] D. Thonig, J. Henk, and O. Eriksson, Gilbert-like damping caused by time retardation in atomistic magnetization dynamics, *Phys. Rev. B* **92**, 104403 (2015).
- [67] L. Thomas, M. Hayashi, X. Jiang, R. Moriya, C. Rettner, and S. S. P. Parkin, Oscillatory dependence of current-driven magnetic domain wall motion on current pulse length, *Nature* **443**, 197 (2006).
- [68] L. Thomas, M. Hayashi, X. Jiang, R. Moriya, C. Rettner, and S. S. P. Parkin, Resonant amplification of magnetic

- domain-wall motion by a train of current pulses, *Science* **315**, 1553 (2007).
- [69] L. Thomas, R. Moriya, C. Rettner, and S. S. P. Parkin, Dynamics of magnetic domain walls under their own inertia, *Science* **330**, 1810 (2010).
- [70] J.-Y. Chauleau, R. Weil, A. Thiaville, and J. Miltat, Magnetic domain walls displacement: Automotion versus spin-transfer torque, *Phys. Rev. B* **82**, 214414 (2010).
- [71] T. Taniguchi, K.-J. Kim, T. Tono, T. Moriyama, Y. Nakatani, and T. Ono, Precise control of magnetic domain wall displacement by a nanosecond current pulse in Co/Ni nanowires, *Appl. Phys. Express* **8**, 073008 (2015).
- [72] A. Pivano and V. O. Dolocan, Systematic motion of magnetic domain walls in notched nanowires under ultrashort current pulses, *Phys. Rev. B* **96**, 224431 (2017).
- [73] B. Gaury, J. Weston, M. Santin, M. Houzet, C. Groth, and X. Waintal, Numerical simulations of time-resolved quantum electronics, *Phys. Rep.* **534**, 1 (2014).
- [74] F. Mahfouzi, B. K. Nikolić, and N. Kioussis, Antidamping spin-orbit torque driven by spin-flip reflection mechanism on the surface of a topological insulator: A time-dependent nonequilibrium Green function approach, *Phys. Rev. B* **93**, 115419 (2016).
- [75] N. Bode, L. Arrachea, G. S. Lozano, T. S. Nunner, and F. von Oppen, Current-induced switching in transport through anisotropic magnetic molecules, *Phys. Rev. B* **85**, 115440 (2012).
- [76] F. Mahfouzi and B. K. Nikolić, How to construct the proper gauge-invariant density matrix in steady-state nonequilibrium: Applications to spin-transfer and spin-orbit torques, *SPIN* **3**, 1330002 (2013).
- [77] S. E. Barnes and S. Maekawa, Generalization of Faraday's Law to Include Nonconservative Spin Forces, *Phys. Rev. Lett.* **98**, 246601 (2007).
- [78] Shufeng Zhang and Steven S.-L. Zhang, Generalization of the Landau-Lifshitz-Gilbert Equation for Conducting Ferromagnets, *Phys. Rev. Lett.* **102**, 086601 (2009).
- [79] K. Gilmore, Y. U. Idzerda, and M. D. Stiles, Identification of the Dominant Precession-Damping Mechanism in Fe, Co, and Ni by First-Principles Calculations, *Phys. Rev. Lett.* **99**, 027204 (2007).
- [80] A. Croy and U. Saalman, Propagation scheme for nonequilibrium dynamics of electron transport in nanoscale devices, *Phys. Rev. B* **80**, 245311 (2009).
- [81] B. S. Popescu and A. Croy, Efficient auxiliary-mode approach for time-dependent nanoelectronics, *New J. Phys.* **18**, 093044 (2016).
- [82] B. K. Nikolić, L. P. Zârbo, and S. Souma, Imaging mesoscopic spin Hall flow: Spatial distribution of local spin currents and spin densities in and out of multiterminal spin-orbit coupled semiconductor nanostructures, *Phys. Rev. B* **73**, 075303 (2006).
- [83] J. Weston and X. Waintal, Linear-scaling source-sink algorithm for simulating time-resolved quantum transport and superconductivity, *Phys. Rev. B* **93**, 134506 (2016).
- [84] M. G. Vavilov, V. Ambegaokar, and I. L. Aleiner, Charge pumping and photovoltaic effect in open quantum dots, *Phys. Rev. B* **63**, 195313 (2001).
- [85] M. Moskalets and M. Büttiker, Floquet scattering theory of quantum pumps, *Phys. Rev. B* **66**, 205320 (2002).
- [86] L. E. F. Foa Torres, Mono-parametric quantum charge pumping: Interplay between spatial interference and photon-assisted tunneling, *Phys. Rev. B* **72**, 245339 (2005).
- [87] U. Bajpai, B. S. Popescu, P. Plecháč, B. K. Nikolić, L. E. F. Foa Torres, H. Ishizuka, and N. Nagaosa, Spatio-temporal dynamics of shift current quantum pumping by femtosecond light pulse, arXiv.org/abs/1803.04404.
- [88] A. Singh, S. Mukhopadhyay, and A. Ghosh, Tracking Random Walk of Individual Domain Walls in Cylindrical Nanomagnets with Resistance Noise, *Phys. Rev. Lett.* **105**, 067206 (2010).
- [89] P. Krzysteczko *et al.*, Nanoscale thermoelectrical detection of magnetic domain wall propagation, *Phys. Rev. B* **95**, 220410 (2017).
- [90] D. Wei, M. Obstbaum, M. Ribow, C. H. Back, and G. Woltersdorf, Spin Hall voltages from A.C. and D.C. spin currents, *Nat. Commun.* **5**, 3768 (2014).
- [91] L. Berger, Possible existence of a Josephson effect in ferromagnets, *Phys. Rev. B* **33**, 1572 (1986).
- [92] G. E. Volovik, Linear momentum in ferromagnets, *J. Phys. C: Solid State Phys.* **20**, L83 (1987).
- [93] A. Stern, Berry's Phase, Motive Forces, and Mesoscopic Conductivity, *Phys. Rev. Lett.* **68**, 1022 (1992).
- [94] W. M. Saslow, Spin pumping of current in non-uniform conducting magnets, *Phys. Rev. B* **76**, 184434 (2007).
- [95] R. A. Duine, Spin pumping by a field-driven domain wall, *Phys. Rev. B* **77**, 014409 (2008); R. A. Duine, Effects of nonadiabaticity on the voltage generated by a moving domain wall, *Phys. Rev. B* **79**, 014407 (2009).
- [96] Y. Tserkovnyak and M. Mecklenburg, Electron transport driven by nonequilibrium magnetic textures, *Phys. Rev. B* **77**, 134407 (2008).
- [97] Y. Liu, O. A. Tretiakov, and A. Abanov, Electrical signature of magnetic domain-wall dynamics, *Phys. Rev. B* **84**, 052403 (2011).
- [98] M. E. Lucassen, G. C. F. L. Kruis, R. Lavrijssen, H. J. M. Swagten, B. Koopmans, and R. A. Duine, Spin motive forces due to magnetic vortices and domain walls, *Phys. Rev. B* **84**, 014414 (2011).
- [99] Y. Yamane, J. Ieda, J. Ohe, S. E. Barnes, and S. Maekawa, Equation-of-motion approach of spin-motive force, *J. Appl. Phys.* **109**, 07C735 (2011).
- [100] K. M. D. Hals and A. Brataas, Spin-motive forces and current-induced torques in ferromagnets, *Phys. Rev. B* **91**, 214401 (2015).
- [101] S. A. Yang, G. S. D. Beach, C. Knutson, D. Xiao, Q. Niu, M. Tsoi, and J. L. Erskine, Universal Electromotive Force Induced by Domain Wall Motion, *Phys. Rev. Lett.* **102**, 067201 (2009).
- [102] P. N. Hai, S. Ohya, M. Tanaka, S. E. Barnes, and S. Maekawa, Electromotive force and huge magnetoresistance in magnetic tunnel junctions, *Nature* **458**, 489 (2009); D. C. Ralph, The Electromotive force of MnAs nanoparticles, *Nature* **474**, E6 (2011).
- [103] K. Tanabe, D. Chiba, J. Ohe, S. Kasai, H. Kohno, S. E. Barnes, S. Maekawa, K. Kobayashi, and T. Ono, Spin-motive force due to a gyrating magnetic vortex, *Nat. Commun.* **3**, 845 (2012).
- [104] F. Freimuth, S. Blügel, and Y. Mokrousov, Dynamical and current-induced Dzyaloshinskii-Moriya interaction: Role

- for damping, gyromagnetism, and current-induced torques in noncollinear magnets, [arXiv.org/abs/1806.04782](https://arxiv.org/abs/1806.04782).
- [105] Y. Yamane, J. Ieda, and J. Sinova, Electric voltage generation by antiferromagnetic dynamics, *Phys. Rev. B* **93**, 180408(R) (2016).
- [106] M. B. Jungfleisch, W. Zhang, and A. Hoffmann, Perspectives of antiferromagnetic spintronics, *Phys. Lett. A* **382**, 865 (2018).
- [107] J. Rhensius, L. Heyne, D. Backes, S. Krzyk, L. J. Heyderman, L. Joly, F. Nolting, and M. Kläui, Imaging of Domain Wall Inertia in Permalloy Half-Ring Nanowires by Time-Resolved Photoemission Electron Microscopy, *Phys. Rev. Lett.* **104**, 067201 (2010).
- [108] K. Dolui and B. K. Nikolić, Spin-memory loss due to spin-orbit coupling at ferromagnet/heavy-metal interfaces: *Ab initio* spin-density matrix approach, *Phys. Rev. B* **96**, 220403(R) (2017).
- [109] S. K. Kim and Y. Tserkovnyak, Magnetic Domain Walls as Hosts of Spin Superfluids and Generators of Skyrmions, *Phys. Rev. Lett.* **119**, 047202 (2017).

Correction: The name of the fifth author appeared incorrectly due to a conversion error and has been fixed.